Fully automated planning for anatomical fetal brain MRI on 0.55T

Sara Neves Silva, Sarah Mcelroy, Jordina Aviles Verdera, Kathleen Colford, Kamilah St Clair, Raphael Tomi-tricot, Alena Uus, Valéry Ozenne, Megan Hall, Lisa Story, et al.

HAL Id: hal-04740898
https://hal.science/hal-04740898v1

Submitted on 17 Oct 2024

RESEARCH ARTICLE

Magnetic Resonance in Medicine

Fully automated planning for anatomical fetal brain MRI on 0.55T

Sara Neves Silva[1,2] 🅞 🐦　|　Sarah McElroy[1,3] 🅞　|　Jordina Aviles Verdera[1,2] 🅞　|
Kathleen Colford[1,2]　|　Kamilah St Clair[1,2]　|　Raphael Tomi-Tricot[1,3]　|　Alena Uus[1,2] 🅞　|
Valéry Ozenne[4]　|　Megan Hall[2,5]　|　Lisa Story[2,5]　|　Kuberan Pushparajah[2]　|
Mary A. Rutherford[1,2]　|　Joseph V. Hajnal[1,2]　|　Jana Hutter[1,2,6] 🅞

[1]Centre for the Developing Brain, School of Biomedical Engineering & Imaging Sciences, King's College London, London, UK

[2]Biomedical Engineering Department, School of Biomedical Engineering & Imaging Sciences, King's College London, London, UK

[3]MR Research Collaborations, Siemens Healthcare Limited, Camberley, UK

[4]CNRS, CRMSB, UMR 5536, IHU Liryc, Université de Bordeaux, Bordeaux, France

[5]Department of Women & Children's Health, King's College London, London, UK

[6]Smart Imaging Lab, Radiological Institute, Friedrich-Alexander University Erlangen-Nuremberg, Erlangen, Germany

Correspondence
Sara Neves Silva, Centre for the Developing Brain, School of Biomedical Engineering & Imaging Sciences, King's College London, London, UK
Email: sara.neves_silva@kcl.ac.uk

Abstract

Purpose: Widening the availability of fetal MRI with fully automatic real-time planning of radiological brain planes on 0.55T MRI.

Methods: Deep learning-based detection of key brain landmarks on a whole-uterus echo planar imaging scan enables the subsequent fully automatic planning of the radiological single-shot Turbo Spin Echo acquisitions. The landmark detection pipeline was trained on over 120 datasets from varying field strength, echo times, and resolutions and quantitatively evaluated. The entire automatic planning solution was tested prospectively in nine fetal subjects between 20 and 37 weeks. A comprehensive evaluation of all steps, the distance between manual and automatic landmarks, the planning quality, and the resulting image quality was conducted.

Results: Prospective automatic planning was performed in real-time without latency in all subjects. The landmark detection accuracy was 4.2 ± 2.6 mm for the fetal eyes and 6.5 ± 3.2 for the cerebellum, planning quality was 2.4/3 (compared to 2.6/3 for manual planning) and diagnostic image quality was 2.2 compared to 2.1 for manual planning.

Conclusions: Real-time automatic planning of all three key fetal brain planes was successfully achieved and will pave the way toward simplifying the acquisition of fetal MRI thereby widening the availability of this modality in nonspecialist centers.

KEYWORDS
fetal brain development, fetal MRI, motion correction, motion detection, T2* relaxometry, tracking

1 | INTRODUCTION

MRI plays an increasing role in both clinical antenatal diagnosis and research, complementing ultrasound screening for a range of suspected fetal pathologies. The most common clinical indication[1] for fetal MR imaging is thereby suspected brain anomalies. MRI has demonstrated specific additional utility when compared with ultrasound in evaluating the posterior fossa,[2] midline structures, the cortex in the progressively ossifying fetal skull, evidence of hemorrhage,[3] cysts, cleft palates[4] and head and neck tumors,[5] among others.

MRI offers, complementary to ultrasound, enhanced soft tissue contrast, a wide range of functional contrasts, and generally high spatial resolution. However, it poses unique challenges, such as safety considerations, involuntary fetal motion, artifacts arising from air–tissue boundaries, and variability in fetal position and maternal surroundings. The most widely used acquisition technique is T2-weighted two-dimensional single-shot Turbo Spin Echo (ssTSE), providing excellent contrast and an in-plane resolution of 1–1.5 mm, while effectively freezing motion for each individual slice.

Radiological assessment requires high-quality images in a set of defined fetal brain planes to perform a set of key measurements including the bi-parietal diameter, trans-cerebellar diameter, and ventricle diameters among others, and to visualize essential structures like the corpus callosum[6] and cerebellar vermis to identify deviations from normal development. Furthermore, gyrification and cortical development may be visualized in detail. Given the size of the studied structures, the accuracy of these measurements is crucial and relies on the availability of exact sagittal, coronal, and axial slices. While recent advances in Slice-to-Volume-Reconstruction[7–10] allow three-dimensional (3D) reconstructed high-resolution 3D volumes and thus re-orientation to true brain anatomy in cases where suboptimal, oblique native planes are acquired, this technique is currently only available in specialist centers and often performed offline. Specialized radiographers trained to perform this challenging planning for fetal MRI are essential. Typically, acquisition planning is performed by optimizing the angles manually and iteratively on stacks acquired in different orientations such as whole uterus sagittal and coronal ssTSE sequences.

Another recent development is the rediscovery of low-field 0.55T MRI. It addresses some of the aforementioned challenges of fetal MRI: the increased field homogeneity reduces distortion artifacts, the larger bore size widens access to pregnant women with larger body mass index, and in later gestation, the reduced heating allows more efficient acquisitions and the longer T2* is beneficial for widely performed T2* relaxometry measurements. Recent studies showed its benefits as a promising tool for fetal MRI.[11–13] The reduced cost, footprint, and eliminated need for shimming tools particularly carry the potential to widen access to this modality. However, a careful balance between these benefits and maintenance of adequate image quality given the reduced signal-to-noise ratio (SNR) is required and often leads to a choice of thicker slices to increase the SNR. Thicker slices, however, put further emphasis on accurate planning.

Recent work highlighted the use of AI methods during the acquisition in motion detection, correction, and automatic planning. Specifically in fetal MRI, work showed the ability to perform quality control,[14] automatic segmentation,[15,16] and automatic tracking.[17,18] Automatic field-of-view prescription was shown in the abdomen using deep learning segmentations[19] and in the heart using tracking based on landmarks[20] with successful detection ratings of 99.7%–100% for cine images and Euclidean distances between manual and automatically detected labels from 2 to 3.5 mm. Similar work in the brain detecting landmarks such as the anterior and posterior commissures and subsequently the symmetry line using multitask deep neural networks were demonstrated among others by Yang et al.[21] Specifically for fetal MRI, segmentation of the eye region and detection of the general head position was suggested by Hoffmann et al.[22] using classical image processing methods such as maximally stable extremal regions and by Xu et al.[23] using convolutional networks—both applicable for real-time slice planning in the future.

Here, we present an automatic, fast landmark detection and subsequent automatic radiological planning of fetal brain scans. The technique was implemented, tested, and evaluated on prospective 0.55T low-field fetal MRI scans.

2 | METHODS

A method allowing automatic planning of the three radiological fetal brain planes using landmarks is presented and compared to manual planning. The methods section will first detail the conventional manual planning and then describe the proposed new method.

2.1 | Manual planning of brain acquisitions

Planning radiological fetal brain planes typically requires whole uterus ssTSE acquisitions as a starting point. An example is given in Figure 1. The orbits of the eyes
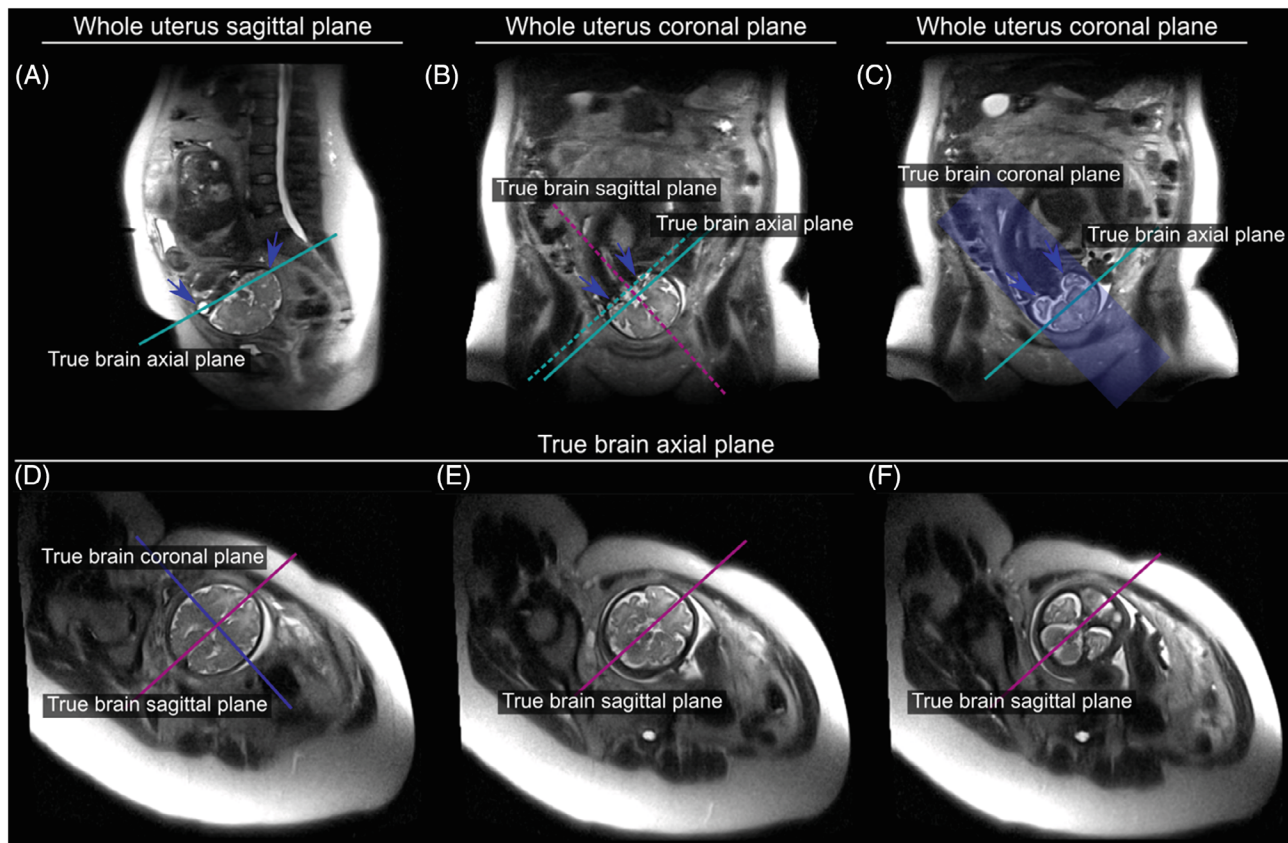
FIGURE 1 Conventional manual planning of the three radiological orientations for fetal anatomical T2-weighted single-shot turbo spin echo (ssTSE) acquisitions. (A–C) illustrate whole uterus ssTSE slices in sagittal and coronal orientation to the uterus overlaid with the planning lines (cyan) to obtain (D) an axial brain ssTSE stack, allowing together with the uterus stacks to plan true sagittal (pink planning lines) and coronal (dark blue planning lines) brain ssTSE stacks. The blue arrows in A–C illustrate the used landmarks during manual planning.

and the back of the skull (Figure 1A, blue arrows) are used to define the orientation of the true brain axial scan, with final adjustments accomplished using the bottom of the lobes (Figure 1B, blue arrows, dotted blue line), slightly shifting the center of the acquisition toward the center of the brain (Figure 1B, blue line showing through-plane view). The midline between the two hemispheres allows to guide the true brain sagittal orientation (Figure 1B, dotted pink line, through-plane view). A favorable view of the lobes is shown in Figure 1C, which is subsequently used to define the true brain coronal acquisition (blue box, in-plane view). After the true brain axial scan is acquired, final adjustments to the coronal and sagittal radiological planes are performed, for instance by checking that the sagittal center of acquisition matches the brain midline across multiple axial slices (Figure 1D–F, pink lines showing sagittal through-plane view). The dotted lines show preliminary planning and the full lines show the final planning of the scan.

2.2 | Automatic planning of brain acquisitions

The automatic sequence planning framework was implemented on a 0.55T scanner (MAGNETOM Free.Max, Siemens Healthcare). A whole-uterus multi-echo gradient-echo single-shot echo planar imaging (EPI) sequence in coronal maternal orientation is acquired in less than 30 s to perform T2* mapping in several fetal organs and the placenta. In this study, this sequence is additionally used for the automatic detection of fetal brain structures that enable automatic planning. The proposed solution consists of three steps: (A) The fetal brain position is detected on the EPI scan and a bounding box is generated, (B) The landmarks in the fetal head are identified, (C) The true fetal brain planes are calculated and applied to the following high-resolution ssTSE sequences (see Figure 2 for an overview of the process and Table 1 for all used imaging parameters).
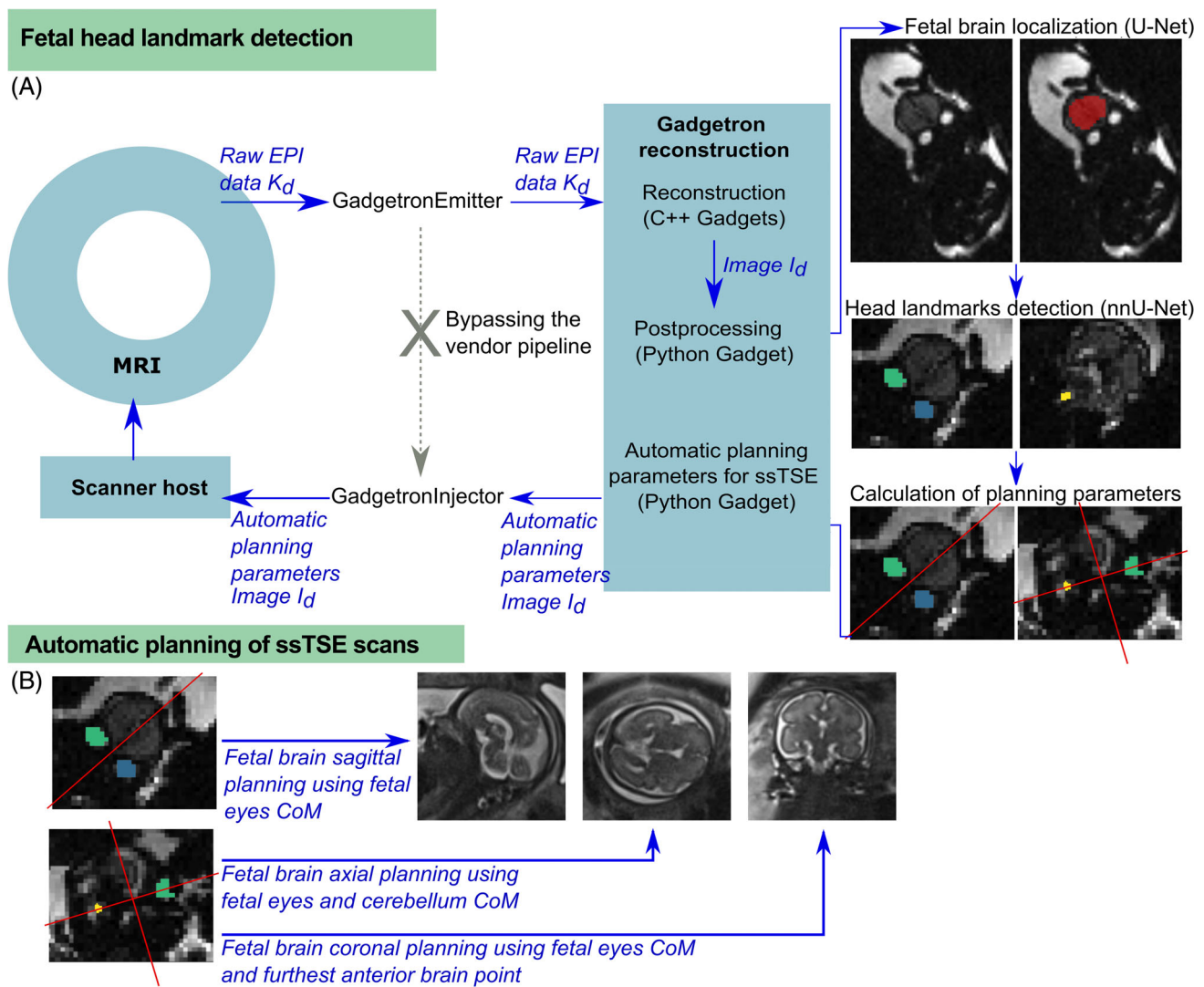
FIGURE 2 Schematic overview over the entire pipeline for automatic planning. (A) Detection of the fetal brain landmarks in the echo planar imaging sequence and (B) Planning parameters applied in the single-shot turbo spin echo sequence.

TABLE 1 Sequence parameters for all described sequences used for training (first two rows, white) and for the prospective automatic planning method (last two rows, gray).

Dataset	Parameters		Subjects	Time
EPI training 1.5T	1.5T Philips Ingenia, 28-channel torso coil			
	Matrix = 144×144–288×288, Resolution 2.5 mm isotropic, 30–96 slices			
	TE = [14.6/77.4/140.1/202.8/265.5] ms, TR = 6.4-23 s		80	22.5 s
EPI training 3T	3T Philips Achieva, 32-channel cardiac coil			
	Matrix = 144×144-192×192, Resolution 2/3 mm isotropic, 45–75 slices			
	TE = [3.8/70.4/127/183.6] / [10.1/54.3/98.4/142.5/186.8] ms, TR = 18.4-23.1 ms		77	18.3 s
EPI autoplan	0.55T Siemens MAGNETOM Free.Max, 6-channel coil, 9-channel spine coil			
	Matrix = 100×100–128×128, Resolution 3.13–4.0 mm isotropic			
	TE = 81 ms, 50–59 slices, TR = 24.5–29 s		9	25 s
ssTSE autoplan	0.55T Siemens MAGNETOM Free.Max, 6-channel coil, 9-channel spine coil			
	Matrix = 304×304, Resolution $1.48 \times 1.48 \times 4.5$ mm^3, 35 slices			
	TE = 106 ms, TR = 14.6 s		9	55 s

Abbreviations: EPI, echo planar imaging; ssTSE, single-shot turbo spin echo; TE, echo time.

2.3 | Localization of the fetal brain

First, the EPI sequence was modified to export the acquired raw data to a Gadgetron reconstruction pipeline,[24] deployed on an external GPU-equipped (NVIDIA GEFORCE RTX 2080 Ti, NVIDIA Corporate) computer connected to the internal network of the MRI scanner. The raw data is converted to ISMRMRD format immediately upon acquisition and reconstructed using off-the-shelf Gadgets that provide generic modules for configuring the streaming reconstruction in the Gadgetron framework. Then, a Python Gadget was implemented to automatically estimate the position of the region of interest in the image using a pretrained 3D UNet[25] for fetal brain localization. A bounding box encompassing the fetal brain is calculated and used for the following landmark detection task.[18]

2.3.1 | Datasets and training

The fetal brain localization network was trained on 125 labeled fetal EPI datasets acquired at 1.5T/3T and tested on 29 0.55T fetal datasets. To increase the robustness of the network, the EPI scans used for the training and performance evaluation of the model deliberately vary in the acquisition parameters (field strength, echo time, resolution, acceleration factor), gestational age (15–40 weeks), fetal health (control cases, fetal growth restriction, prolonged preterm rupture of the membranes, etc.), and fetal position (cephalic, breech, transverse). The parameters for the training data set were: (1) 3T Philips Achieva, 32-channel cardiac coil and 16-channel spine coil, matrix size $= 144 \times 144$–192×192, isotropic resolution $2\,mm^3$, TE $= [3.8/70.4/127/183.6]/[10.1/54.3/98.4/142.5/186.8]$ ms, 45–75 slices; (2) 1.5T Philips Ingenia, 28-channel torso coil, matrix size$=144 \times 144$–288×288, isotropic resolution 2.5 mm, TE $= [14.6/77.4/ 140.1/202.8/265.5]$ ms, 30–96 slices. The trained model was tested on low-field fetal datasets acquired on a 0.55T Siemens MAGNETOM Free.Max, using a blanket-like BioMatrix Contour-L 6-channel coil and fixed 9-channel spine coil, matrix size $= 100 \times 100$–128×128, isotropic resolution 3.13–4.0 mm, TE $= [46/120/194/268/342]$ ms, 50–59 slices.

2.4 | Landmark detection

A deep learning-based landmark detection method using the nnUNet framework[26] was adopted to extract specific head landmarks, concretely the orbit of both fetal eyes and the lower edge of the cerebellum. This framework performs semantic segmentation and it automatically adapts to a given dataset by analyzing the provided training data and configuring a matching UNet-based segmentation pipeline. Furthermore, the furthest anterior point (FAP) of the fetal brain mask is extracted. The center of mass (CoM) coordinates of the landmarks, the brain mask, and the FAP are then transformed into the patient coordinate system and written into a text file on the external server and scanner host. Figure 3A illustrates the key points extracted and used for planning the radiological acquisitions.

2.4.1 | Datasets and training

The landmark nnUNet was trained and tested on cropped and labeled low-field EPI images of 76/15 fetal subjects, respectively. Automatic cropping was performed to the 0.55T whole-uterus coronal EPI scans by first applying the inference of the fetal brain localization network to the datasets and using the estimated fetal brain position to define a bounding box that is defined by the brain mask and an expansion factor of 50%, defining how much the bounding box should be enlarged relative to the dimensions of the fetal brain, ensuring that the cropped region contains all key landmarks. The cropped images defined by the fetal head bounding boxes were therefore used as input for the training and testing of the landmark detection network. The gold standard segmentations of the landmarks were manually drawn for each dataset. All slice stacks were acquired using the low-field fetal protocol described above.

2.5 | Calculation of the radiological brain planes

2.5.1 | Automatic orientation calculation of brain acquisitions

The ssTSE sequence that follows the EPI sequence in the protocol was modified to use the information stored in the autoplan file, which includes the landmarks and fetal brain CoM coordinates and FAP, to calculate the three standard radiological planes axial, sagittal, and coronal. The normal vector to the sagittal plane is calculated as the vector between the eyes landmarks (see Figure 3B). It was identified that the eyes and FAP lie on the same approximately coronal plane and the eyes and cerebellum lie on the same approximately axial plane. Therefore, the normal vector to the coronal plane was calculated as the dot product of the two vectors between each eye and the FAP,

(A)

(B)
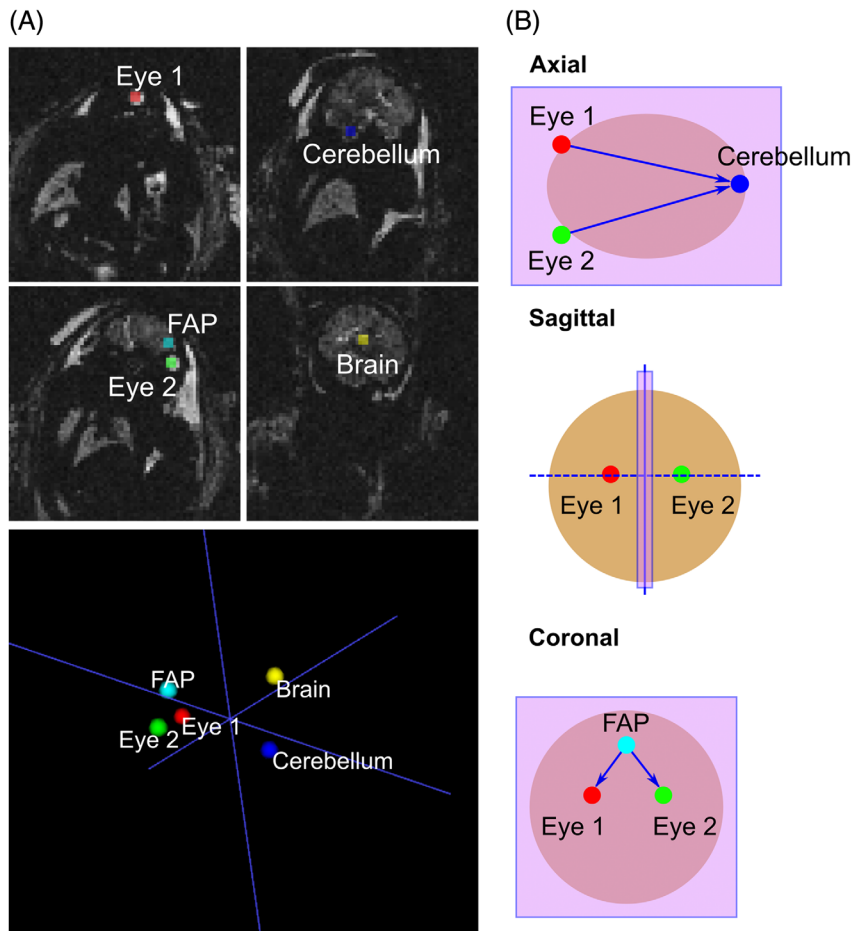
FIGURE 3 (A) Key points extracted from the whole-uterus coronal echo planar imaging (EPI) scan for automatic planning of the single-shot turbo spin echo (ssTSE) scans are illustrated: these include key landmarks eyes (red and green dots) and cerebellum (blue dot) and two points extracted from the fetal brain: the brain center of mass (CoM, yellow dot) and the furthest anterior point. (B) The axial orientation is defined using the eyes and cerebellum center of mass coordinates, the sagittal orientation uses the eyes CoM coordinates, and the coronal orientation is defined using the eyes CoM and furthest anterior point of the fetal brain mask. The brain CoM is used to define the center of the slice stack for all radiological planes. The purple boxes illustrate the slice position for each orientation: in axial and coronal planes the views shown are in-plane, and for the sagittal plane the view shown is through-plane.

and the normal vector to the axial plane as the dot product of two vectors between each eye and the cerebellum. A hierarchical approach is chosen to increase robustness even more: If the cerebellum is not extracted successfully, the CoM of the brain is used instead for the vector calculation. The CoM of the brain is used to define the center of the slice stack for all planes.

2.6 | Experiments and evaluation

2.6.1 | Evaluation of the fetal brain localization and landmark detection accuracy

The performance of the localization network was analyzed using the dice similarity coefficient and the Intersection-over-Union metric calculated between the gold standard manual segmentations performed by two fetal experts (9 and 2 years of fetal MRI experience, respectively) and the brain masks generated by the network. The landmark detection performance was analyzed by calculating the 3D distance between the center of mass of the manual segmentations of the landmarks performed by fetal MRI experts and the landmarks obtained from the network.

2.6.2 | Real-time fetal brain plane planning

The entire pipeline was acquired prospectively in nine pregnant volunteers in St Thomas' Hospital, recruited between October and December 2023 after informed consent was obtained as part of two ethically approved studies (MEERKAT REC19/LO/0852 and miBirth 23/LO/0685). Women were scanned on the above-described clinical 0.55T MAGNETOM Free.Max scanner in the supine position with leg support to ensure comfort with life monitoring throughout the scan. Gestational ages ranged between 20.3 and 37.3 weeks (mean 32.8 ± 3.5). For each fetal subject, the initial whole-uterus coronal multi-echo gradient-echo single-shot EPI scan was acquired (resolution = 3.13–4.0 mm isotropic, TE=[81/227/372] ms, 50–59 slices, matrix size = 128 × 128). Subsequently, the automatically-planned ssTSE (autoplan-ssTSE) prototype sequence was acquired in all three radiological planes with the following parameters: resolution = 1.48 × 1.48 × 4.5 mm³, TE = 106 ms, 35 slices, matrix size = 304 × 304, TE = 106 ms, TR = 14.6 s. In addition, the same sequence was acquired with manual planning of the three radiological planes by fetal radiographers (1–5 years of experience) for all subjects. In total, for each fetal subject, three planes (axial, coronal, and sagittal) were acquired,

resulting in a total of 27 acquisitions of each planning approach—manual and automatic. The time required for planning by the radiographers and the automatic method was measured.

2.6.3 | Evaluation of the planning quality and diagnostic quality of the prospectively acquired images

Quantitative evaluation was performed blinded to the method and the ability to produce accurate measures was scored. The resulting automatically planned radiological planes were assessed by a fetal radiographer with 5 years of fetal MRI experience answering the questions "Rate the planning quality [1-3]" (1 – re-acquisition required, 2 – usable, 3 – full brain coverage, symmetry of the brain structures, no re-acquisition required). A fetal radiologist with >15 years of experience additionally quantified the clinical value of the automatic planning method by attempting to perform, for both manually and automatically planned acquisitions, five measurements in the sagittal view (corpus callosum, cerebellar vermis, pons anterior-posterior (AP) diameter, pituitary stalk, hard palate), four in the coronal view (trans-cranial diameter [TCD], bi-parietal diameter [BPD], cavum septum pellucidum, ventricle) and five in the axial view (BPD, occipito-frontal diameter [OFD], ventricle, TCD, cavum septum pellucidum). The radiologist was asked to answer "Can you perform all radiological measurements? [0-5]" (0 – unusable, 5 – all five measurements successfully performed). The results were in addition assessed against gestational age and maternal body mass index.

3 | RESULTS

3.1 | Fetal brain localization

The brain localization task, trained on mid/high-field data, achieved an overall dice similarity coefficient of 0.82 ± 0.18 and intersection-over-union of 0.73 ± 0.19 when tested on low-field scans across all TEs, fetal positions, and gestational ages. Extraction of fetal brain masks took between 11.4 and 20.6 ms per volume in the offline testing mode.
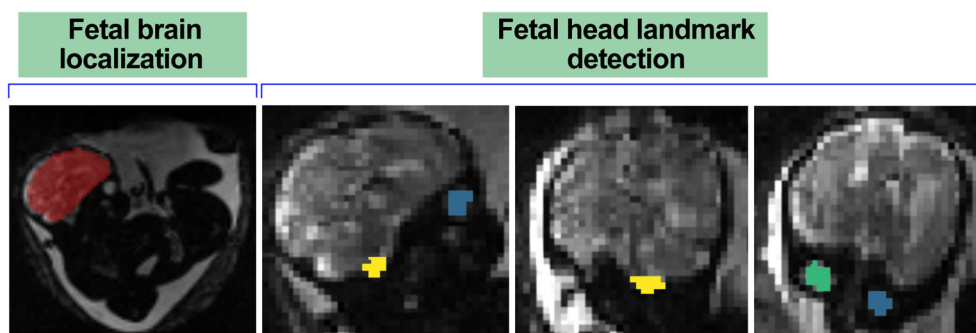
3.2 | (B) Landmark detection

The mean distance between the CoM of the eyes and cerebellum labels from automatic and manual segmentations was 4.2 ± 2.6 mm and 6.5 ± 3.2 mm, respectively. Figure 4 shows the predicted brain and landmarks segmentations for one fetal subject of the landmarks model test set. Figure 5 shows examples of predicted landmarks generated by the nnUNet, the corresponding ground-truth segmentations, and the distance between the two. Landmark detection took 5.2 s per volume in the offline testing mode.

3.3 | Real-time fetal brain plane planning

The entire pipeline was successfully run in all nine fetal scans, with all steps of the approach successfully implemented and tested prospectively. The estimated time between the completion of the EPI sequence and the start of the ssTSE sequence, ready to be run with the planning parameters correctly set, is less than 5 s with the automatic method, and an average of 1.5 min for the specialist radiographer and 4 min for the novice radiographer. Landmark detection and automatic radiological planning are shown in Figure 6 alongside the radiographer's manually planned acquisitions, with matching anatomical structures in the manual and automatic acquisitions highlighted to demonstrate that both techniques allow the same structures of interest to be captured comparably. The anatomies (green squares, blue arrows) are labeled between 1 and 10, with the corresponding dictionary at the bottom.

FIGURE 4 Two-step localisation task—global localization of the fetal head using a fetal brain segmentation three-dimensional UNet model, and local localization with extraction of the three fetal head landmarks—eyes and cerebellum.
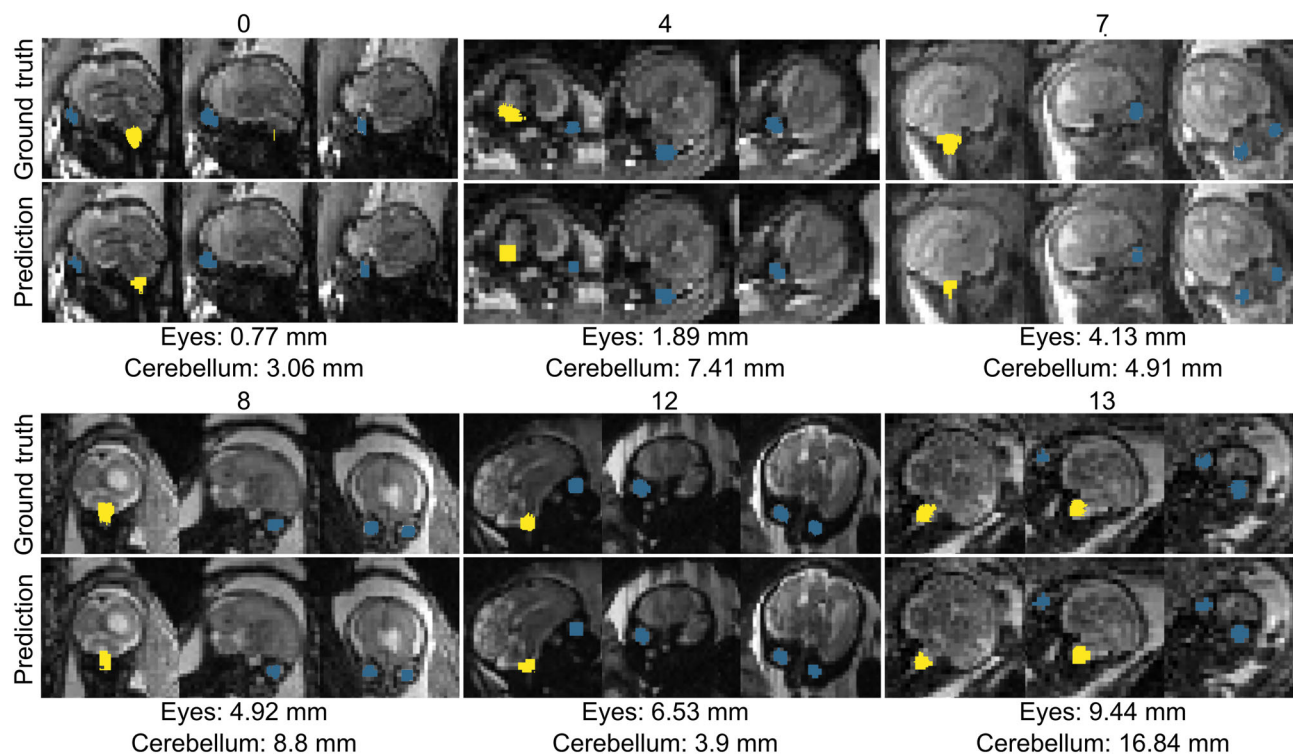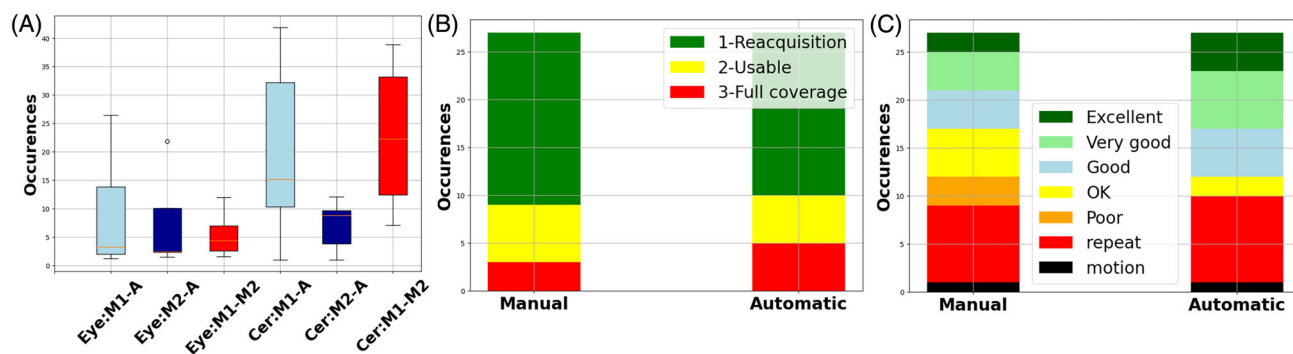
FIGURE 5 Ground-truth and predicted landmarks, generated by the nnUNet, for fetal subjects 0, 4, 7, 8, 12, and 13 of the landmark detection test set. The distance between the center of mass of each is additionally displayed. The model outputs the eyes landmarks using a single label, hence they are depicted with the same color (and label). This result is then processed to separate the two unconnected regions to be used to guide the planning of the single-shot turbo spin echo scan.

In Figure 7A, a quantitative assessment of the real-time landmark detection task applied to the prospective whole uterus EPI scans is depicted. The landmarks were extracted in real-time during the scan to automatically plan the radiological brain acquisitions and were subsequently segmented manually by two observers M1 and M2, where M2 is the observer that segmented the landmarks for training the nnUNet. All landmarks but one cerebellum segmentation (fetal subject 9 of Gestational age [GA] 20 weeks) were prospectively extracted during the scan. The inability of the model to extract the landmark may be linked to the early gestation of the fetus and the consequent small size of the brain structures, as well as the fact that early gestation fetuses are not as well represented in the training dataset of the model, a natural bias that is often present in fetal MRI studies. For this case, the CoM of the brain was used instead as a landmark to allow for the automatic planning to still be performed. For the nine fetal subjects scanned, the differences in distances (in mm) between the CoM of eyes and cerebellum landmarks segmented by M1, M2, and automated (A) were calculated. For the eyes, the difference between M1 and A ranged between 1.3 and 21.8 mm, M2-A between 1.5 and 10.1 mm, and M1-M2 between 1.5 and 12.0 mm. As for the cerebellum, the CoM differences in distance for M1-A

ranged between 9.4 and 41.9 mm, M2-A between 2.0 and 12.1 mm, and M1-M2 between 7.1 and 38.9 mm. While inter-observer variability never exceeded 11.98 mm for the eyes landmarks, the cerebellum presented much larger variability in the segmentations produced by M1 and M2, which can be explained by the boundaries of this anatomical structure not being as well defined as for the eyes, leading to variability in the size of the segmentation. For this reason, using a deep learning approach helps to eliminate observer bias, as segmentations are more standardised and consistent.

The quantitative evaluation of the three achieved radiological planes is displayed in Figures 7B,C and 8. In both figures, the assessments performed by the radiographer and radiologist aimed to score how close to a perfect true brain plane each acquisition was and the clinical value of the automatically planned images (compared with the manually planned ones). With three radiological planes (axial, coronal, and sagittal) acquired for each fetal subject, 27 planes were acquired in total in this work. Out of 27 automatically planned acquisitions, 22 scans were successfully acquired without the need for re-acquisition, and 24 out of 27 manually planned scans similarly did not require repeating according to the analysis performed by a fetal radiographer. Full brain coverage was achieved

1 Posterior horns of the lateral ventricles
2 Frontal horns of the lateral ventricles
3 Cavum septum pellucidum
4 Cerebellum
5 Pons
6 Superior sagittal sinus
7 Lateral ventricles
8 Medulla oblongata
9 Straight sinus
10 Cisterna magna

FIGURE 6 Landmarks extracted from whole uterus coronal echo planar imaging (EPI) scans and radiographer-planned and automatic (orientation defined from the position of the eyes and cerebellum, extracted from the EPI) radiological single-shot turbo spin echo acquisitions. Anatomical structures of interest were highlighted (green squares, blue arrows) for manual and automatic acquisitions to demonstrate comparable orientation planning.

FIGURE 7 Quantitative evaluation of the 27 prospectively acquired single-shot turbo spin echo (ssTSE) datasets. (A) Landmark assessment: Difference in mm between the manual segmentations performed by two observers (M1 and M2) and the automatic method (A) for the eyes and the cerebellum. (B) Radiographer assessment: Image quality for all 27 acquisitions for the manual and automatic acquisitions. (C) Radiologist assessment: Image quality for all 27 acquisitions for the manual and automatic acquisitions.

in all radiological planes for all manual and automatic scans, thus the need for re-acquisition resided in large tilts present in the orientation of the brain, with asymmetries visible between the two brain hemispheres and anatomical structures of interest present in both.

In 27 manually planned scans, six scans displayed slight asymmetry with small rotations of the anatomy that would not affect the clinical value of the images and thus did not require re-acquisition (four coronal planes and two axial). Severe asymmetry was observed in three acquisitions (two axial planes and one sagittal) with re-acquisition needed. The remaining 18 acquisitions showed a complete symmetry of the two brain hemispheres. Regarding the automatic planning method, full symmetry of the brain hemispheres and neurological structures was achieved in 17 automatic acquisitions, demonstrating the ability of the method to plan true brain planes accurately. Generating the automatic acquisition plane took, on average, 5 s, and the radiological acquisitions were acquired in less than one minute each. Asymmetry was observed in 10 cases, although at different degrees: five scans showed larger asymmetry with severe tilts (three axial planes, one coronal, and one sagittal), and five showed smaller tilts causing slight asymmetry which would not affect the clinical value of acquisitions and therefore would not require re-acquisition (two coronal planes, two sagittal, and one axial). Figure 7B illustrates the radiographer assessments. In summary, a quality score of 81.5% (2.4/3) was achieved by the automatic planning method and 85.2% (2.6/3) for manual planning. Further details of the planning quality assessment can be found in Appendix S1.

The clinical value and image quality were additionally evaluated by a fetal radiologist. With a maximum score of 14 measurements per fetal subject, the number of measurements successfully performed in the manually

planned acquisitions was: 14, 10, 7, 6 (two subjects), five (two subjects, 1 of GA 20 weeks), two, and one. Artifacts were also visible in three coronal acquisitions, which may have affected the ability to perform measurements. Using the automatic planning method, the number of measurements performed was: 12, 11 (two subjects), seven (one plane showing artifacts), five (two subjects), four (fetal subject of GA 20 weeks), three, and zero (one plane showing distortion). An average of 2.07/5 measurements were successfully performed by a radiologist for the manual acquisitions, and 2.14/5 for the automatic acquisitions.

The measurements with the highest scores across all fetal subjects and all orientations were the cavum septum pellucidum and the ventricle, in the coronal orientation, with scores of manual 8/9 and automatic 6/9 subjects for both measurements. The corpus callosum (manual 1/9, automatic 0/9 subjects) and pons AP diameter (manual 1/9, automatic 2/9 subjects), both in sagittal orientation, showed the lowest scores. For both sagittal and coronal orientations, radiographer-planned acquisitions scored slightly higher than the automated ones (by 2.2% and 5.0%, respectively); however, the automatically planned axial orientation was superior to the manual planning by 11.1%. Overall, the automatic method for planning the acquisitions was 1.6% higher than the manual planning approach, according to the image quality quantitative assessment performed by a radiologist.

As illustrated in Figure 7C, out of 27 manual scans five measurements were performed in two scans, four measurements in four scans, three in four scans, two in five scans, one in three scans, and one dataset severely affected by motion, resulting in eight scans without immediate clinical value (unless tools for rotating the brain anatomy are utilized). This motion corruption of the ssTSE scans
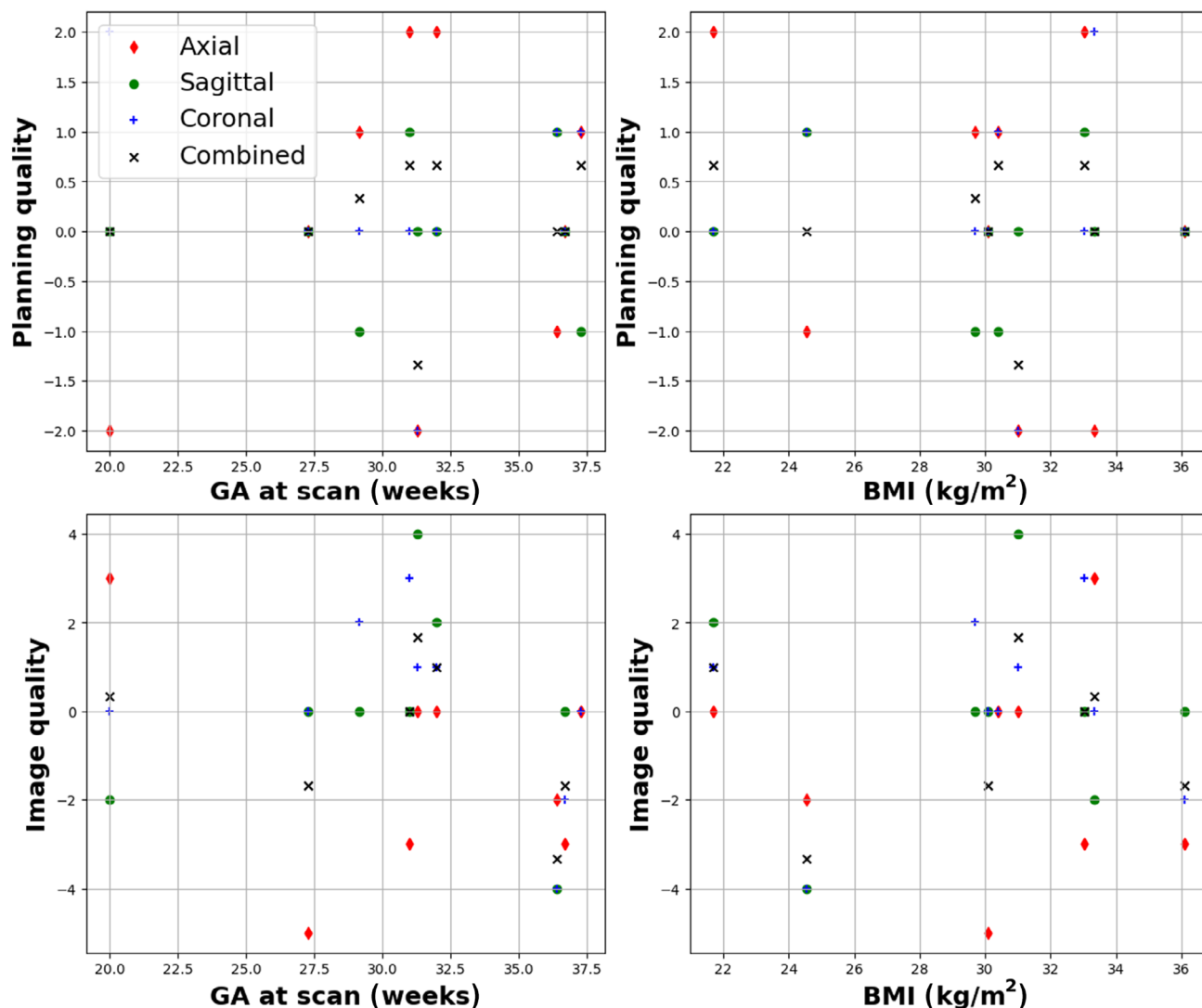
FIGURE 8   Quantitative assessment of the planning quality (A,B) and image quality (C,D) illustrated for all three planes (coronal, axial, and sagittal) against GA (A, C) and maternal body mass index (B, D). The plotted values correspond to the difference between the manual and automatic planning quality (for A,B) and image quality (for C,D) scores: positive values indicate, for the same plane, greater quality of the manual orientation, negative values indicate a greater quality of the automated acquisitions and 0 for the cases where both manual and automated acquisitions showed matched quality.

during the automatic planning task refers to the instances where the fetus was actively moving during the image acquisition, resulting in signal dropouts in the brain region in many of the slices and causing the images to not hold diagnostic value unless volumetric reconstruction is performed. Regarding the automatically planned scans, five measurements were performed in four scans, four measurements in six scans, three in five scans, and two in two scans. One dataset was similarly corrupted by motion, resulting in nine scans without immediate clinical value.

Figure 8 depicts planning quality, assessed by a radiographer, and image quality, assessed by a radiologist, according to gestational age (GA at scan) and maternal body mass index.

4 | DISCUSSION AND CONCLUSION

In this study, a fully automated framework for planning all three radiological fetal brain planes was demonstrated in low-field MRI scans. The method presented uses a whole-uterus coronal multi-echo EPI sequence, acquired and employed for T2* relaxometry, to serve the additional purpose of fetal head landmark detection. The brain and key landmarks are automatically extracted and handed to the subsequent ssTSE acquisition to plan fetal brain-oriented acquisitions in under 5 s. This automatic planning of fetal MRI scans, shown here as comparable to the manual planning for clinical reporting, reduces

dependence on specialist staff and increases time efficiency and thus carries the potential to significantly widen accessibility to fetal MRI beyond specialist centers.

In line with recent work,[22] the eyes were successfully used as landmarks and were crucial for calculating the orientation of the fetal brain, however, the detection shown here did not include further pose estimation or image processing steps. While recent work employing AI to detect landmarks and organs on the MR acquisitions focused on 1.5T and 3T,[14,18,20,22,23,27] the present work was performed on low field fetal MRI at 0.55T, providing increasing challenges regarding SNR and resolution, but allowing to take key steps toward wider accessibility of fetal MRI.

The retrospective evaluation of the network that extracts the head landmarks (eyes and cerebellum) resulted in an average distance between the CoM of the manually segmented and automatically extracted eyes of 4.2 mm, which corresponds to 1.3 voxels, and 6.5 mm for the cerebellum, corresponding to 2.1 voxels, thus it is sufficiently robust for the calculation of the radiological planes. Fetal subjects 8 and 13 of the test set showed the largest distances (mm) between the CoM of manual and automatic landmark masks, however, Figure 5 demonstrates how even at such large distances (9.4 and 16.8 mm for eyes and cerebellum of Fetus 13) the predictions are still highly comparable to the gold standard segmentations and extract the key landmarks accurately enough for the orientation calculations of the ssTSE scans. According to the quantitative and qualitative assessments of the calculation of the radiological brain planes, the automatically planned scans achieved comparable image quality to the scans manually planned by an experienced fetal radiographer. Regarding the fetal brain localization task, which uses a network trained on 1.5T/3T data and applied to 0.55T acquisitions, it is only required for cropping the whole-uterus images to the fetal head. Therefore, the brain segmentations do not require high precision and accuracy but only need to offer sufficient information for the first-step localization, which was demonstrated in all retrospective and prospective cases.

Major strengths of the current study are the complete and robust real-time deployment. The two-step approach presented here for landmark detection: first the identification of the brain with a 3D UNet followed by the landmark detection using nnUNet and the hierarchical application of landmarks in cases where individual landmarks are not identified—for example, replacing the cerebellum by the center of the brain for the sagittal prescription—contributes to robustness even in younger fetuses. Furthermore, the developed method was built using open-source frameworks, facilitating straightforward translation and dissemination.

There are, however, limitations with the current study. First, the present study is a single-center study. The training data and retrospectively assessed test data are small, as well as the number of prospective cases, which currently does not allow a more robust evaluation of the method in a larger cohort. This is often the case in fetal MRI as such a modality is not yet widely available worldwide and data sharing policies between institutions and studies are often restrictive. The framework may need to be further refined to perform robustly in wider populations and across different scanners/field strengths. Future work will hence investigate further developments to ensure the robustness of the automatic planning framework in this wider context. EPI images are reconstructed using standard Fourier reconstruction computed with off-the-shelf Gadgets (without image filtering or AI-based image enhancement provided by the scanner reconstruction pipeline) resulting in limited SNR, which may hinder the performance of the landmark detection. This will be addressed by further improving the real-time reconstruction pipeline, by including image filtering or AI-based image enhancement to achieve increased SNR in the EPI images. Fetal MRI at higher field will suffer less from this limitation. Although dice similarity coefficient and intersection-over-union were used to evaluate the performance of the fetal brain localization network, these metrics present limitations, especially in the presence of outliers and imbalanced data. Failure metrics, such as the (weighted) sum of false positives and false negatives are often recommended as these can provide a more comprehensive performance evaluation by focusing on directly measuring the segmentation errors. Figure 7A depicts how the cerebellum, as a region in the fetal brain with very low contrast and not well-defined boundaries, especially in EPI acquisitions, can lead to high segmentation inter-observer variability. The manual segmentations used for training the landmarks network were produced by observer M2, hence the network demonstrated a bias toward such cerebellar masks. In this case, the use of a network can help stabilize the segmentation task—by integrating segmentations from multiple observers during the network training, observer variability, and bias can be reduced and the model can produce standardized segmentations based on this training information. Next, this framework is based on a whole-uterus multi-echo EPI sequence, not requiring any planning and fitting to the standard patient examination as current practice for all fetal MRI scans in our institution. However, the reduced resolution of this EPI sequence (3 mm isotropic) compared to the ssTSE sequence (1.25 mm in-plane) might influence the achieved precision regarding landmark detection. The network and achieved complete automatic planning can, however, be extended to whole uterus ssTSE localiser scans in the future. Furthermore, while the landmarks

were chosen as independently as possible from brain structures involved in common pathologies such as the ventricles and the corpus callosum—and in line with recent work[22]—the automatic planning in fetuses with developmental abnormalities in the location of the lower edge of the cerebellum or the orbits of the eyes might involve the need for additional manual adjustment. Finally, adding a fourth landmark in the back of the skull might be helpful to further stabilize the planning of the acquisition in the axial orientation.

Future work toward an automatic fetal brain MR examination will furthermore include the real-time deployment of automatic quality control,[14] subregional segmentation[10] and automatic biometry.[28]

To conclude, this study shows the feasibility of rapid deep learning-based automatic planning of anatomical radiological fetal brain scans and presents an open-source framework open for further extensions and improvements. The clear next application is fetal cardiac landmark detection for automatic planning of phase contrast sequences acquired to study the flow in the major arteries.

CONFLICT OF INTEREST

Sarah McElroy and Raphael Tomi-Tricot are employees of Siemens Healthineers.

DATA AVAILABILITY STATEMENT

All steps, including the EPI reconstruction with off-the-shelf Gadgets, the fetal brain localization and landmark detection trained models, and Gadget are available to any interested researchers (https://github.com/saranevessilva/fetal-brain-landmarks). All anonymized fetal data is also available upon request.

ORCID

Sara Neves Silva 🄳 https://orcid.org/0009-0009-7520-081X
Sarah McElroy 🄳 https://orcid.org/0000-0002-4271-5931
Jordina Aviles Verdera 🄳 https://orcid.org/0009-0007-7575-4244
Alena Uus 🄳 https://orcid.org/0000-0001-5796-2145
Jana Hutter 🄳 https://orcid.org/0000-0003-3476-3500

TWITTER

Sara Neves Silva 🐦 saranevessilva

REFERENCES

1. Alford RE, Bailey AA, Twickler DM. Fetal central nervous system. In: Masselli G, ed. *MRI of Fetal and Maternal Diseases in Pregnancy*. Springer; 2016:91-118. doi:10.1007/978-3-319-21428-3_6
2. Prayer D, Brugger PC, Nemec U, Milos RI, Mitter C, Kasprian G. Cerebral malformations. In: Prayer D, ed. *Fetal MRI. Medical Radiology*. Springer; 2010:287-308. doi:10.1007/174_2010_117
3. Epstein KN, Kline-Fath BM, Zhang B, et al. Prenatal evaluation of intracranial Hemorrhage on Fetal MRI: a retrospective review. *Am J Neuroradiol*. 2021;42:2222-2228. doi:10.3174/ajnr.A7320
4. van der Hoek-Snieders HEM, van den Heuvel AJML, van Os-Medendorp H, Kamalski DMA. Diagnostic accuracy of fetal MRI to detect cleft palate: a meta-analysis. *Eur J Pediatr*. 2020;179:29-38. https://link.springer.com/article/10.1007/s00431-019-03526-7
5. Cornejo P, Feygin T, Vaughn J, et al. Imaging of fetal brain tumors. *Pediatr Radiol*. 2020;50:1959-1973. doi:10.1007/s00247-020-04777-z
6. Kyriakopoulou V, Vatansever D, Davidson A, et al. Normative biometry of the fetal brain using magnetic resonance imaging. *Brain Struct Funct*. 2017;222:2295-2307. doi:10.1007/s00429-016-1345-8.
7. Gholipour A, Rollins CK, Velasco-Annis C, et al. A normative spatiotemporal MRI atlas of the fetal brain for automatic segmentation and analysis of early brain growth. *Sci Rep*. 2017;7:476. https://www.nature.com/articles/s41598-017-00516-6
8. Uus A, Zhang T, Jackson LH, et al. Deformable slice-to-volume registration for motion correction of Fetal body and placenta MRI. *IEEE Trans Med Imaging*. 2020;39:2750-2759. doi:10.1109/TMI.2020.2972867
9. Kuklisova-Murgasova M, Quaghebeur G, Rutherford MA, Hajnal JV, Schnabel JA. Reconstruction of fetal brain MRI with intensity matching and complete outlier removal. *Med Image Anal*. 2012;16:1550-1564. doi:10.1016/j.media.2012.06.001
10. Uus AU, Kyriakopoulou V, Makropoulos A, et al. BOUNTI: brain vOlumetry and aUtomated parcellatioN for 3D feTal MRI. *bioRxiv*. 2023;27:2023.04.18.537347. doi:10.1101/2023.04.18.537347

11. Aviles Verdera J, Story L, Hall M, et al. Reliability and feasibility of low-field-strength Fetal MRI at 0.55 T during pregnancy. *Radiology*. 2023;309:e223050. doi:10.1148/radiol.223050

12. Ponrartana S, Nguyen HN, Cui SX, et al. Low-field 0.55 T MRI evaluation of the fetus. *Pediatr Radiol*. 2023;53:1469-1475. doi:10.1007/s00247-023-05151-8

13. Payette K, Uus A, Aviles Verdera J, et al. An automated pipeline for quantitative T2* fetal body MRI and segmentation at low field. *ArXiv*. 2023 https://arxiv.org/abs/2308.02132

14. Gagoski B, Xu J, Wighton P, et al. Automated detection and reacquisition of motion-degraded images in fetal HASTE imaging at 3 T. *Magn Reson Med*. 2022;87:1914-1922. doi:10.1002/mrm.29106

15. Faghihpirayesh R, Karimi D, Erdogmus D, Gholipour A. Deep learning framework for real-time fetal brain segmentation in MRI. *arXiv* 2022 https://arxiv.org/abs/2205.01675

16. Salehi SSM, Hashemi SR, Velasco-Annis C, et al. Real-time automatic fetal brain extraction in fetal MRI by deep learning. Paper presented at: 2018 IEEE 15th International Symposium on Biomedical Imaging (ISBI 2018); April. 2018:720-724. doi:10.1109/ISBI.2018.8363542

17. Singh A, Salehi SSM, Gholipour A. Deep predictive motion tracking in magnetic resonance imaging: application to Fetal imaging. *IEEE Trans Med Imaging*. 2020;39:3523-3534. doi:10.1109/TMI

18. Neves Silva S, Aviles Verdera J, Tomi-Tricot R, et al. Real-time fetal brain tracking for functional fetal MRI. *Magn Reson Med*. 2023;90:2306-2320.

19. Lei K, Syed AB, Zhu X, Pauly JM, Vasanawala SV. Automated MRI field of view prescription from region of interest prediction by intra-stack attention neural network. *Bioengineering (Basel)*. 2023;10(1):92. doi:10.3390/bioengineering10010005

20. Xue H, Artico J, Fontana M, Moon JC, Davies RH, Kellman P. Landmark detection in cardiac MRI by using a convolutional neural network. *Radiol Artif Intell*. 2021;3(5):e200197.

21. Yang X, Tang WT, Tjio G, Yeo SY, Su Y. Automatic detection of anatomical landmarks in brain MR scanning using multi-task deep neural networks. *Neurocomputing*. 2020;396:514-521. doi:10.1016/j.neucom.2020.04.078

22. Hoffmann M, Abaci Turk E, Gagoski B, et al. Rapid head-pose detection for automated slice prescription of fetal-brain MRI. *Int J Imaging Syst Technol*. 2021;31:1136-1154. doi:10.1002/ima.22563

23. Xu J, Zhang M, Turk EA, et al. Fetal pose estimation in volumetric MRI using a 3D convolution neural network. *Med Image Comput Comput Assist Intervent*. 2019;2019:403-410.

24. Hansen MS, Sørensen TS. Gadgetron: an open source framework for medical image reconstruction. *Magn Reson Med*. 2013;69:1768-1776. doi:10.1002/mrm.24383

25. Uus A, Grigorescu I, van Poppel M, et al. 3D UNet with GAN discriminator for robust localization of the fetal brain and trunk in MRI with partial coverage of the fetal body. *bioRxiv*. 2021;2021-2026. doi:10.1101/2021.06.23.449574

26. Isensee F, Jaeger PF, Kohl SAA, Petersen J, Maier-Hein KH. nnU-net: a self-configuring method for deep learning-based biomedical image segmentation. *Nat Methods*. 2021;18:203-211. doi:10.1038/s41592-020-01008-z

27. Mohseni Salehi SS, Khan S, Erdogmus D, Gholipour A. Real-time deep pose estimation with geodesic loss for image-to-template rigid registration. *IEEE Trans Med Imaging*. 2019;38:470-481. doi:10.1109/TMI.2018.2866442

28. She J, Huang H, Ye Z, et al. Automatic biometry of fetal brain MRIs using deep and machine learning techniques. *Sci Rep*. 2023;13:17860. doi:10.1038/s41598-023-17202-0

SUPPORTING INFORMATION

Additional supporting information may be found in the online version of the article at the publisher's website.

Appendix S1. Supporting information.

How to cite this article: Neves Silva S, McElroy S, Aviles Verdera J, et al. Fully automated planning for anatomical fetal brain MRI on 0.55T. *Magn Reson Med*. 2024;92:1263-1276. doi: 10.1002/mrm.30122